Event-Based Model Predictive Control Framework for Joint Reliability and Energy Optimization in Bus Operations

Assaf Granot* and Jack Haddad

Technion–Israel Institute of Technology, Faculty of Civil and Environmental Engineering
Postal address: Technion City, Rabin building, Room 726, Israel. Phone: +972 77 8871742,
jh@technion.ac.il

Short summary

Most existing studies on bus transport systems treat service reliability and operational sustainability as separate objectives. This paper presents an integrated simulation and optimal control framework that jointly addresses both. We develop a real-time, event-based simulation environment that captures human-driven bus behavior under realistic traffic conditions, passenger demand, and operational disturbances, calibrated using open-source data. Building on this platform, we design and implement two complementary control strategies within a Model Predictive Control (MPC) framework: holding control at stops and speed limit regulation. The controllers are jointly optimized to regulate time headways while minimizing energy consumption. The framework is evaluated on five high-frequency bus lines in the Tel Aviv metropolitan area. Simulation results show that the combined strategy reduces headway deviations by over 60% while achieving approximately 15% reductions in total energy consumption. These results demonstrate that jointly designed, minimally intrusive control strategies can simultaneously improve reliability and sustainability in urban bus operations.
Keywords: Energy Efficiency, Model Predictive Control, Public Transport Operation, Service Reliability

1 Introduction

In response to climate change and urban pollution, the transportation sector faces increasing pressure to adopt low-emission alternatives. Air pollution, noise, and space constraints highlight the need for public transportation systems that are attractive, sustainable, and reliable. Buses, the most widely used public transport mode (UITP, 2017), offer significant potential in this transition (Borén, 2020). Operating on fixed routes, buses, particularly electric ones, provide a scalable solution for urban decarbonization. However, without effective operational management, bus systems may become unstable and unreliable (C. Daganzo, 1997). This paper investigates how real-time operational control can simultaneously improve the reliability and energy efficiency of high-frequency bus systems.

The control of bus systems has been the subject of extensive research. Numerous strategies have been proposed to address service reliability issues. In the literature, these strategies are typically formulated as real-time control methods (Ibarra-Rojas et al., 2015). A central manifestation of operational instability is bus bunching, where vehicles scheduled at regular intervals arrive in close succession, increasing passenger waiting times and operational inefficiencies. In high-frequency services, reliability is therefore often addressed through headway-based control, which prioritizes maintaining regular vehicle intervals rather than strict timetable adherence. Control strategies can generally be grouped into three categories. *Station-level control* includes holding (Zolfaghari et al., 2004; Xuan et al., 2011), boarding limitation (Delgado et al., 2012), and stop-skipping (Cao & Ceder, 2019). *Inter-station control* includes transit signal priority (Christofa & Skabardonis, 2011; Anderson & Daganzo, 2020) and speed control (C. F. Daganzo & Pilachowski, 2011; Sirmatel & Geroliminis, 2018). *Line-level control* includes short-turning, deadheading (Cortés et al., 2011), and timetable optimization (Tang et al., 2020).

Advances in sensing and communication technologies, including Automatic Vehicle Location (AVL) and Automatic Passenger Counting (APC) systems, have enabled the implementation and evaluation of such strategies using simulation and optimization tools (Chen et al., 2024), with control

approaches ranging from classical feedback controllers to Model Predictive Control (MPC) formulations (C. F. Daganzo & Pilachowski, 2011; Sirmatel & Geroliminis, 2018; Varga et al., 2019; Lacombe et al., 2021).

Energy consumption in bus operations has also received significant attention. Previous studies show that vehicle mass, drivetrain characteristics, roadway conditions, and driving behavior strongly influence energy use and emissions (Zhang et al., 2014; Yu et al., 2016). For electric buses, micro-consumption models typically incorporate aerodynamic drag, rolling resistance, road grade, inertial effects, and regenerative braking (Henning, 2008; Armenta-Déu & Cortés, 2023; Xu et al., 2011). However, these models are often developed independently of service reliability considerations. Only a limited number of studies integrate energy consumption within real-time bus control frameworks, and existing work typically relies on simplified operational settings or short simulation horizons (Lacombe et al., 2021, 2020; Varga et al., 2019).

Despite extensive research on bus control and energy modeling, few studies jointly address service reliability and energy efficiency within a unified operational framework. When both objectives are considered, studies are often restricted to simplified system representations or a limited set of control strategies. This paper addresses this gap by developing an event-based MPC framework for bus operations that jointly accounts for reliability and energy consumption under realistic conditions. As illustrated in Fig. 1, the proposed framework targets human-driven operations, where control decisions are issued at stop-arrival events and remain compatible with existing practices. The strategies are evaluated in a data-calibrated simulation environment capturing passenger dynamics, capacity constraints, traffic variability, and fixed operational headways based on real-world data. Holding control, speed-limit control, and their combination are evaluated across multiple case studies.

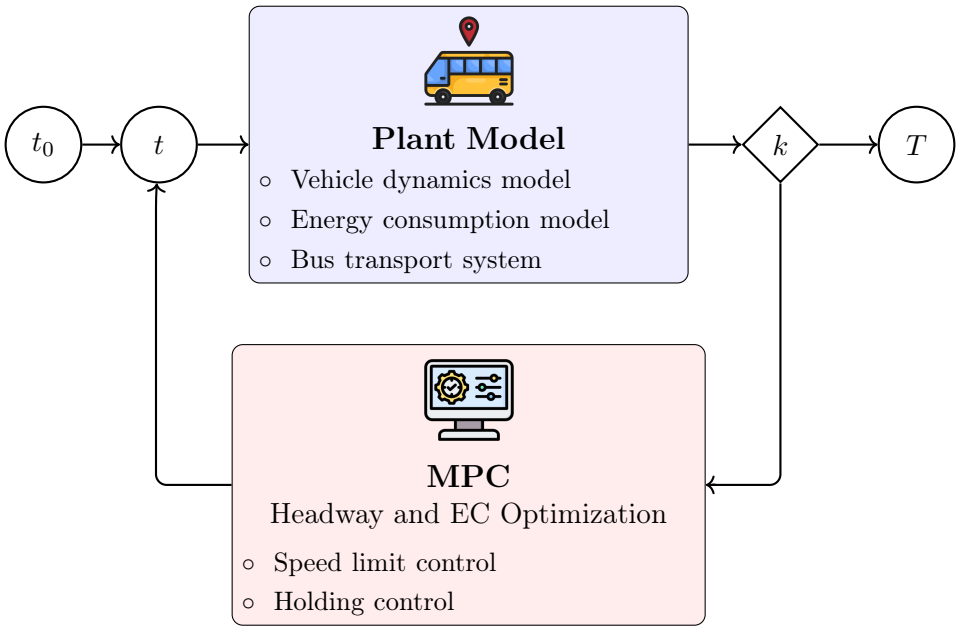


Figure 1: Event-based MPC framework for bus transport systems. Control decisions are triggered at stop-arrival events k, where the MPC computes holding times and segment-wise speed-limit recommendations and feeds them back to the plant model.

2 Methodology

In this section, we develop the MPC framework for bus transport systems illustrated in Fig. 1. The framework combines four components: vehicle dynamics, energy consumption, bus operations, and control. The framework is implemented in Python and MATLAB and calibrated using open-source data collected over the past four years by the Israeli Ministry of Transport and Road Safety. The data include vehicle location records in the SIRI-VM format (European Committee for Standardization (CEN), 2015), stop-level passenger boarding and alighting counts, and planned route information, including stop locations and elevations, in the GTFS format (Google and the GTFS Community, 2024).

Vehicle dynamics model

Following (Newell, 2002; Tuchner & Haddad, 2017), we model the longitudinal dynamics of a fleet of n buses using the state vector $X(t) = [x_1(t), \ldots, x_n(t),\, v_1(t), \ldots, v_n(t),\, a_1(t), \ldots, a_n(t)]^\top$. For each bus $i \in \mathbb{I}_{[1,n]}$, the quantities $x_i(t)$ [m], $v_i(t)$ [m/s], and $a_i(t)$ [m/s^2] denote the position, velocity, and acceleration, respectively. Buses are initially indexed by departure order, and indices are updated dynamically to reflect their longitudinal order along the route. The motion of each bus evolves according to the discrete-time dynamics

$$x_i(t+1) = x_i(t) + \Delta t\, v_i(t) + \frac{\Delta t^2}{2} a_i(t), \tag{1}$$

$$v_i(t+1) = \gamma v_i(t) + (1-\gamma) V_i(\tau), \tag{2}$$

$$a_i(t+1) = \frac{v_i(t+1) - v_i(t)}{\Delta t}, \tag{3}$$

where t is the simulation time step, Δt is the sampling interval, and the parameter $\gamma \in [0,1]$ captures the driver's response to traffic conditions. The target speed $V_i(\tau)$ [m/s] represents the stochastic traffic state experienced by bus i and is updated every τ seconds, an interval chosen to reflect realistic fluctuations in traffic conditions.

Traffic variability along each road segment $(s, s+1)$ is modeled using a segment-specific autoregressive speed process calibrated from historical AVL data. For each segment, the empirical mean speed $\overline{v}_{s,s+1}$ [m/s] and variance $\sigma^2_{s,s+1}$ [m^2/s^2] are estimated from observed travel speeds. Let

$$\epsilon_{s,s+1}(\tau) \sim \mathcal{N}(0, \sigma^2_{s,s+1}) \tag{4}$$

represent stochastic fluctuations in speed around the empirical mean. The traffic state evolves according to

$$V_i(\tau) = \max\Big(0,\, \min\big(SL_{s,s+1},\, \theta\, \overline{v}_{s,s+1} + (1-\theta) V_i(\tau-1) + \epsilon_{s,s+1}(\tau)\big)\Big), \tag{5}$$

where $SL_{s,s+1}$ [m/s] is the segment speed limit and $\theta \in [0,1]$ controls the persistence of the traffic state by balancing the historical mean speed with the previously realized state. The truncation ensures that simulated speeds remain within the feasible range $[0, SL_{s,s+1}]$.

Overtaking is permitted in the model. Bus indices are therefore updated dynamically whenever $x_i(t) > x_{i-1}(t)$. A virtual leading vehicle (bus 1) defines the boundary conditions for headway computation and is not controlled.

Energy consumption model

Following (Asamer et al., 2016; Heydari et al., 2018), bus energy consumption is modeled based on longitudinal dynamics and roadway characteristics. The total driving resistance force of bus i is

$$F_{\mathrm{t},i}(t) = F_{\mathrm{r},i}(t) + F_{\mathrm{w},i}(t) + F_{\mathrm{g},i}(t) + F_{\mathrm{j},i}(t), \tag{6}$$

where the four components represent rolling resistance, aerodynamic drag, gradient resistance, and acceleration resistance. Rolling resistance is modeled as

$$F_{\mathrm{r},i}(t) = m_i(t)\, g\, C_{\mathrm{rr}} \cos(\alpha), \tag{7}$$

where $m_i(t)$ [kg] is the total mass of bus i, g [m/s^2] is gravitational acceleration, C_{rr} [-] is the rolling resistance coefficient, and α [-] is the road slope angle. The aerodynamic drag force is

$$F_{\mathrm{w},i}(t) = \frac{1}{2} \rho C_{\mathrm{D}} A v_i^2(t), \tag{8}$$

where ρ [kg/m^3] is air density, C_{D} [-] is the drag coefficient and A [m^2] is the vehicle frontal area. Gradient resistance is

$$F_{\mathrm{g},i}(t) = m_i(t)\, g\, \sin(\alpha), \tag{9}$$

while acceleration resistance is

$$F_{\mathrm{j},i}(t) = m_i(t)\, a_i(t). \tag{10}$$

The instantaneous traction power of bus i, denoted $P_i(t)$ [W], is obtained from the product of total resistance force and vehicle speed. Energy losses and recovery are represented through drivetrain efficiencies η_{M} [-] for propulsion and η_{G} [-] for regenerative braking. The resulting power model is

$$P_i(t) = \begin{cases} \dfrac{v_i(t)}{\eta_{\mathrm{M}}} F_{\mathrm{t},i}(t), & F_{\mathrm{t},i}(t) \geq 0, \\ \eta_{\mathrm{G}}\, v_i(t) F_{\mathrm{t},i}(t), & F_{\mathrm{t},i}(t) < 0,\ v_i(t) > 3 \text{ m/s}, \\ 0, & F_{\mathrm{t},i}(t) < 0,\ v_i(t) \leq 3 \text{ m/s}. \end{cases} \tag{11}$$

At very low speeds ($v_i(t) \leq 3$ m/s), regenerative braking is assumed ineffective. The cumulative energy consumption of bus i, denoted $E_i(t)$ [Wh], is obtained by integrating power over time:

$$E_i(t) = \int_{t_0}^{T} P_i(t)\, \mathrm{d}t. \tag{12}$$

Because the proposed framework operates in an event-based manner, energy consumption is evaluated for each bus over the trajectory segments between consecutive stop-arrival events.

Bus transport system modeling

The Bus Transport System model captures passenger dynamics, vehicle loads, and stop-level interactions along a bus line. We consider a single line with n buses $i \in \mathbb{I}_{[1,n]}$ serving m stops $s \in \mathbb{I}_{[1,m]}$. Each stop has a predefined location l_s [m], measured along the route trajectory, and the set of stop locations is denoted $L = [l_1, \ldots, l_m]^\top$. We introduce an event index k, triggered for bus i when the vehicle reaches stop s, i.e., when $x_i(t) \geq l_s$ at time $t \triangleq T_i(k)$. Operational variables are updated only at these stop-arrival events.

Time headway Headway regularity is evaluated at stop arrivals. The realized time headway between buses i and $i-1$ at event k is

$$H_i(k) = T_i(k) - T_{i-1}(k) \geq 0. \tag{13}$$

Passenger arrival The expected number of passengers waiting at stop s is $\lambda_s H_i(k)$, where λ_s [pax/s] denotes the passenger arrival rate estimated from historical boarding data. In high-frequency services, passengers are assumed to arrive uniformly in time (Luethi et al., 2007).

Passenger accumulation Passenger boarding and alighting determine the onboard load of bus i, denoted $n_i(k)$ [pax]. The accumulation dynamics are

$$n_i(k) = \lambda_s H_i(k) + (1 - \mu_s) n_i(k-1), \tag{14}$$

where $\mu_s \in [0, 1]$ represents the historical proportion of passengers alighting at stop s. The resulting load must satisfy

$$0 \leq n_i(k) \leq n_{\max}. \tag{15}$$

Dwell time Following (Tirachini, 2013), dwell time is modeled as a function of boarding and alighting activity:

$$t_{\mathrm{d},i}(k) = 5 + 2\big(\lambda_s H_i(k) + \mu_s n_i(k-1)\big), \tag{16}$$

where $t_{\mathrm{d},i}(k)$ [s] denotes the dwell time at stop s. The constant term accounts for door operations and clearance time, while the variable component scales with passenger movements.

Bus mass The mass of bus i depends on the empty vehicle mass and passenger load:

$$m_i(k) = m_{\mathrm{emp}} + n_i(k) m_{\mathrm{pax}}, \tag{17}$$

where m_{emp} [kg] is the empty bus mass and m_{pax} [kg/pax] is the average passenger mass. The mass is bounded by

$$m_{\mathrm{emp}} \leq m_i(k) \leq m_{\mathrm{full}}, \qquad m_{\mathrm{full}} = m_{\mathrm{emp}} + n_{\max} m_{\mathrm{pax}}. \tag{18}$$

Binary states Discrete operational events in the Bus Transport System are represented using binary state variables that indicate whether a bus reaches a stop, serves passengers, or proceeds to the next segment. The logical relationships between these states are illustrated in Fig. 2.

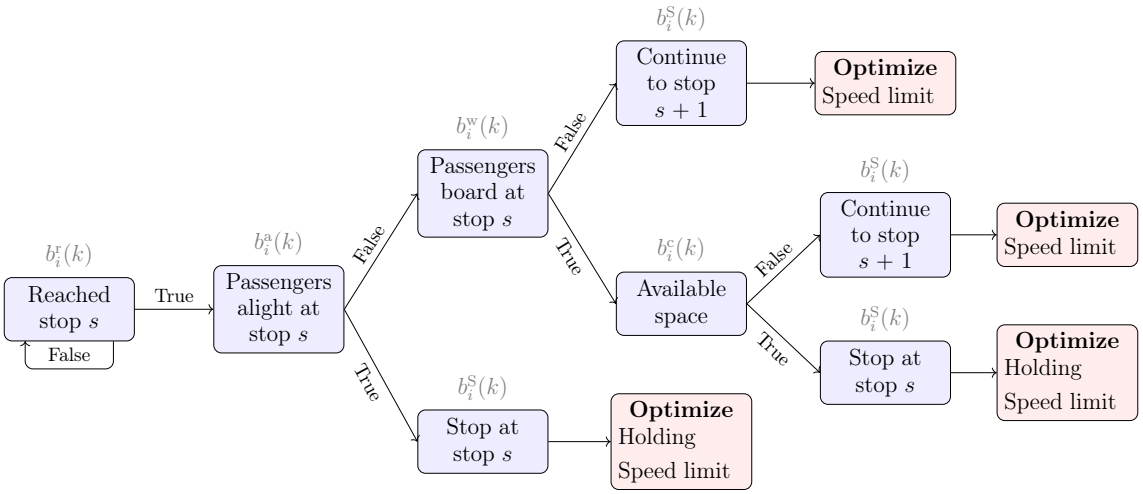


Figure 2: Bus Transport System modeling - binary states for bus i.

Based on these conditions, the model determines whether bus i stops at stop s:

$$b_i^{\mathrm{S}}(k) = \begin{cases} 1, & b_i^{\mathrm{a}}(k) \ \vee \ (b_i^{\mathrm{w}}(k) \wedge b_i^{\mathrm{c}}(k)), \\ 0, & \text{otherwise.} \end{cases} \tag{19}$$

An optimization event is triggered when bus i completes passenger service at stop s or passes the stop without stopping, after which the controller determines the next operational actions.

Control modeling

We adopt a distributed event-based MPC framework. At event k, the controller solves a local optimization problem for bus i and computes two control inputs over the prediction horizon: the holding time $u_{\mathrm{h},i}(k+\ell)$ [s] at stops and the recommended speed limit $u_{\mathrm{SL},i}(k+\ell)$ [m/s] for the subsequent road segments. The control vector is defined as

$$\begin{aligned} u(k+\ell) &\triangleq \begin{bmatrix} u_{\mathrm{h},i}(k+\ell) \\ u_{\mathrm{SL},i}(k+\ell) \end{bmatrix}, \qquad \ell = 0, \dots, N_{\mathrm{p}} - 1\,, \\ \mathbf{u}(k) &\triangleq \begin{bmatrix} u(k)^\top & u(k+1)^\top & \dots & u(k+N_{\mathrm{p}}-1)^\top \end{bmatrix}^\top. \end{aligned} \tag{20}$$

The controller minimizes a weighted sum of headway deviation and predicted energy consumption. The predicted headway is defined as $\widehat{H}_i(k+\ell) = \widehat{T}_i(k+\ell) - \widehat{T}_{i-1}(k+\ell)$, and the predicted segment energy is $\widehat{E}_i(k+\ell) = \int_{T_i(k+\ell)}^{T_i(k+\ell+1)} P_i(t)\,\mathrm{d}t$. The optimization problem is

$$\begin{aligned} \min_{\mathbf{u}(k)} \quad & \sum_{\ell=0}^{N_{\mathrm{p}}-1} \left[\omega_{\mathrm{HW}} \left(H_{\mathrm{ref}} - \widehat{H}_i(k+\ell) \right)^2 + \omega_{\mathrm{EC}}\, \widehat{E}_i(k+\ell) \right] \\ \text{s.t.} \quad & 0 \le u_{\mathrm{h},i}(k+\ell) \le u_{\mathrm{h}_{\max}}, \qquad \ell = 0, \dots, N_{\mathrm{p}} - 1\,, \\ & u_{\mathrm{SL}_{\min}} \le u_{\mathrm{SL},i}(k+\ell) \le SL_{s+\ell,s+\ell+1}, \qquad \ell = 0, \dots, N_{\mathrm{p}} - 1\,, \\ & \text{system dynamics as defined in (1)–(19).} \end{aligned} \tag{21}$$

The holding-time bound $u_{\mathrm{h}_{\max}}$ [s] limits excessive delay at stops, while the speed control input is bounded below by $u_{\mathrm{SL}_{\min}}$ [m/s] and above by the physical segment speed limit $SL_{s+\ell,s+\ell+1}$ [m/s]. As illustrated in Fig. 3, each bus performs local prediction and optimization upon arriving at a stop. The prediction procedure mirrors the structure of the bus transport simulation but is executed independently over a predefined prediction horizon. Starting from the current system state, the controller propagates the dynamics of the controlled bus forward in time while sampling traffic conditions and updating passenger and dwell-time states according to the models defined in

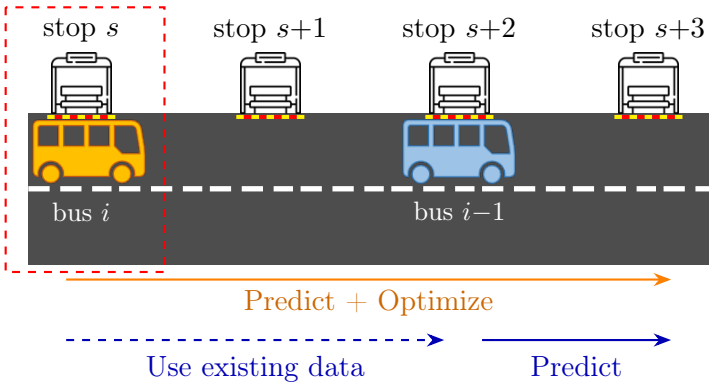


Figure 3: Illustration of event-based MPC with prediction horizons.

Section 2. Because traffic conditions are sampled independently and the traffic process is stochastic, predicted realizations rarely match those later observed by the plant. For all other buses within the prediction range, their known real-time arrival information is used up to the current event, and prediction is performed only from their latest observed stop onward. This enables the computation of the predicted headway $\widehat{H}_i(k+\ell)$ and energy $\widehat{E}_i(k+\ell)$ required for the optimization.
Based on sensitivity analysis, we set the prediction horizon to $N_\mathrm{p} = 3$ events and apply only the first control action, i.e., $N_\mathrm{c} = 1$. The objective weights ω_HW and ω_EC are calibrated to balance the relative magnitudes of the headway and energy terms. The resulting nonlinear optimization problem is solved using Sequential Quadratic Programming (SQP), with multiple randomized initializations to improve robustness against local minima.

3 Results and Discussion

Configuration

The proposed framework was evaluated on five high-frequency bus lines in the Tel Aviv metropolitan area (Fig. 4). The selected lines differ in service frequency, route length, dedicated bus lane (DBL) share, and number of stops, as summarized in Table 1. Some lines operate primarily on DBLs, while others run in mixed traffic, as reflected in historical segment speeds. Given their high frequency and substantial passenger demand, the lines are well-suited to headway-based control. Traffic conditions and demand profiles were estimated for the morning peak (6:00–9:00 AM).

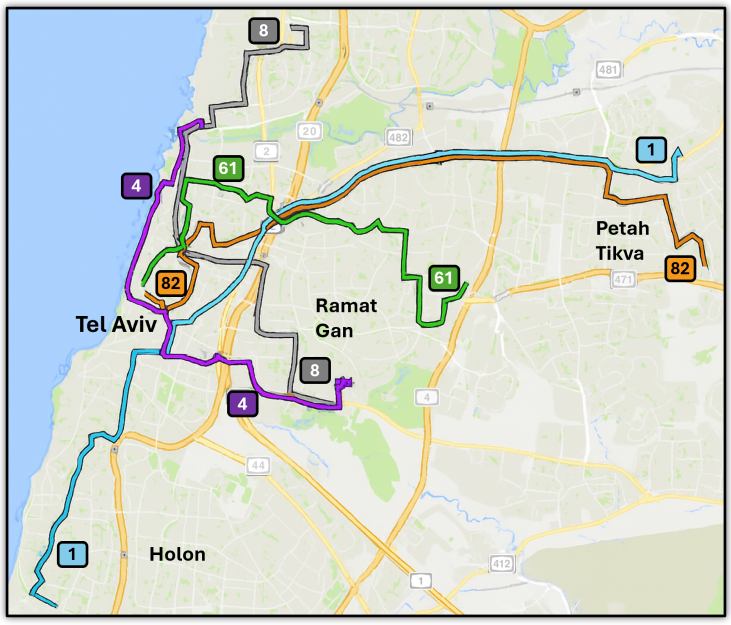


Figure 4: Route layout of the selected bus lines in the Tel Aviv metropolitan area.

Table 1: Examined routes details

Line No.	Freq. [trips/hr]	Length [km]	DBL [%]	No. of Stops
1	6	21.8	93	51
4	10	11.8	34	35
8	8	14.7	38	41
61	6	12.7	18	38
82	10	17.3	61	47

To represent realistic operational disturbances at the terminal, we introduce stochastic variability in departure times, reflecting disruptions such as delayed vehicle arrivals, driver changes, overtime rest breaks, and other uncertainties (Van Oort, 2011). Under ideal conditions, buses depart at regular intervals equal to the planned headway H_{ref} [s]. To generate departure irregularity, a disturbance term e_i [s] is added to the departure time of each bus i. For scenario $j \in \mathbb{I}_{[1,10]}$, the disturbance is modeled as

$$e_i \sim \mathcal{N}(0, \sigma^2_{\text{departure}}), \qquad \sigma_{\text{departure}} = \beta H_{\text{ref}}(j-1), \tag{22}$$

where β [-] is a heuristic scaling parameter controlling the level of variability. As the scenario index j increases, the standard deviation of the disturbance grows proportionally, resulting in progressively less regular departures from the terminal. Simulation parameters and constraint values are listed in Table 2, based primarily on (Gallet et al., 2018; Lacombe et al., 2021; Armenta-Déu & Cortés, 2023), and on data-driven calibration.

Table 2: Parameter assumptions and coefficients used in simulations.

Energy			
Parameter	Notation	Numerical Value	Units
Rolling resistance coefficient	C_{rr}	0.008	[−]
Drag coefficient	C_{D}	0.7	[−]
Gravitational constant	g	9.81	[m/s]
Air density	ρ	1.18	[kg/m^3]
Mass of an empty bus	m_{emp}	12,500	[kg]
Bus's frontal area	A	8.3	[m^2]
Efficiency of driving	η_{M}	0.85	[−]
Efficiency of recuperating	η_{G}	0.75	[−]
Passenger weight	m_{pax}	60	[kg/pax]
Bus Transport System			
Parameter	Notation	Numerical Value	Units
Occupancy boundaries	n_i	[0,80]	[pax]
Simulation time step	Δt	1	[s]
Traffic state updating time	τ	10	[s]
Traffic smoothing coefficient	γ	0.2	[−]
Traffic state balance coefficient	θ	0.6	[−]
Max. holding time allowed	$u_{\text{h}_{\max}}$	20	[s]
Min. Speed limit allowed	$u_{\text{SL}_{\min}}$	0.5·SL	[−]

Performance metrics

Service reliability is evaluated using the coefficient of variation of headways C_{vh} [-] (Associates et al., 2003), defined as

$$C_{\text{vh}} = \frac{\sigma_{\text{HW}}}{H_{\text{ref}}}, \tag{23}$$

where H_{ref} [s] is the planned headway and σ_{HW} [s] is the standard deviation of realized headways. The metric is computed at the stop level and represents service stability using Levels of Service (LoS), from A (reliable operations) to F (severe irregularity and bunching).

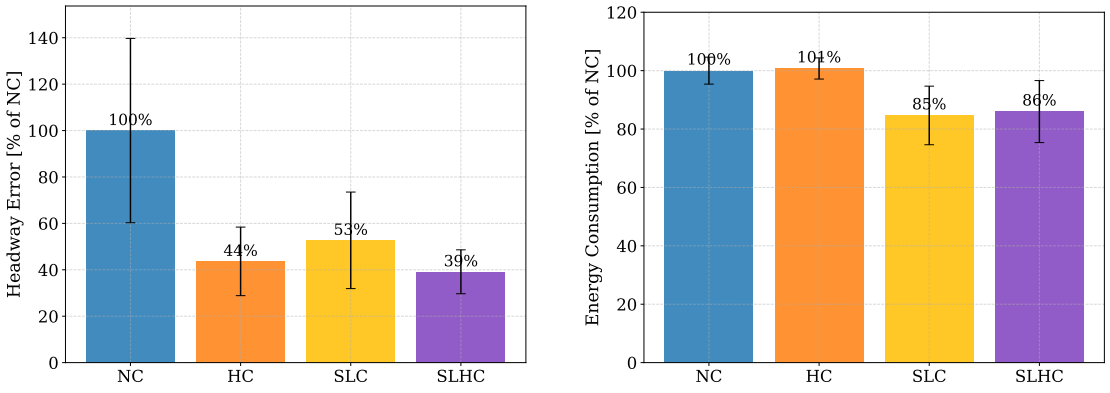
In addition to reliability, we evaluate performance indicators for operators and passengers. From the operator's perspective, total fleet energy consumption (kWh) and average running time are used to assess operational efficiency and potential implications for scheduling and fleet requirements. From the passenger perspective, two time-based indicators are considered: in-vehicle time and waiting time at stops. In-vehicle time reflects the duration passengers spend onboard buses, while waiting time captures the impact of headway variability on passenger delays at stops. As headways become more regular, waiting time decreases accordingly (Ceder, 2016).

Results

Four control strategies are evaluated: No Control (NC), Holding Control (HC), Speed Limit Control (SLC), and the combined Speed Limit & Holding Control (SLHC). Each scenario is simulated 20 times. Scenario 4 ($j = 4$, see (22)), representing moderate departure-time variability consistent with the data, is used for the primary analysis. All performance metrics are reported relative to the NC baseline, normalized to 100%.

Fig. 5 compares the strategies in terms of headway deviation and total energy consumption. The combined strategy SLHC achieves the best reliability performance, reducing headway deviation by 61% relative to NC and outperforming the individual control strategies. In terms of energy, strategies that include speed control yield substantial benefits, reducing total fleet energy consumption by about 15% on average. As illustrated in Fig. 6, these savings arise mainly from smoother speed trajectories that limit strong acceleration and deceleration events. In contrast, HC provides no energy benefit, as expected, since holding does not directly alter the vehicle's speed profile.

Across the analyzed lines, average energy consumption under NC ranged between 1.4 and 1.5 kWh/km, consistent with recent empirical estimates (Würtz et al., 2024).



(a) Mean Headway Error

(b) Total Energy Consumption

Figure 5: Comparison of control strategies for headway error and energy consumption, normalized to the NC baseline.

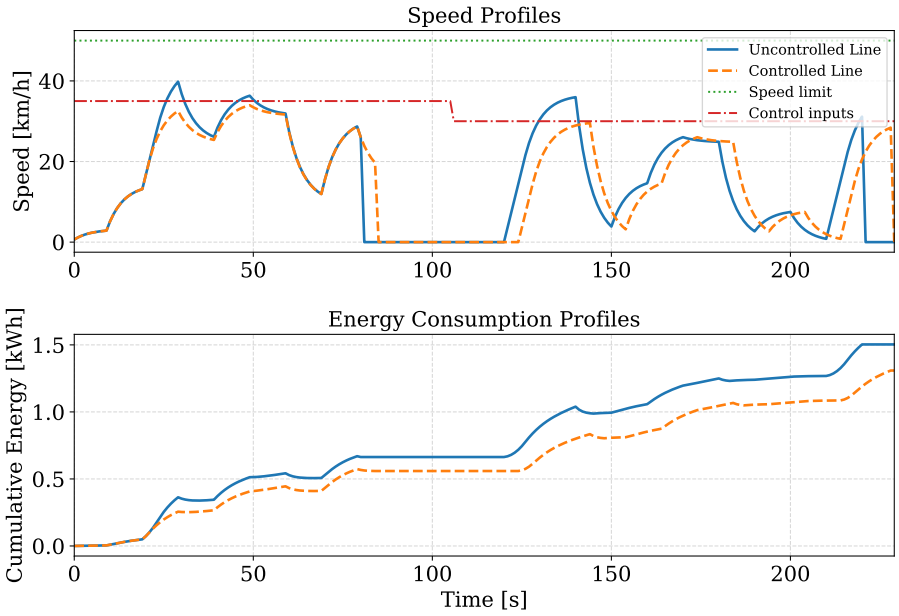
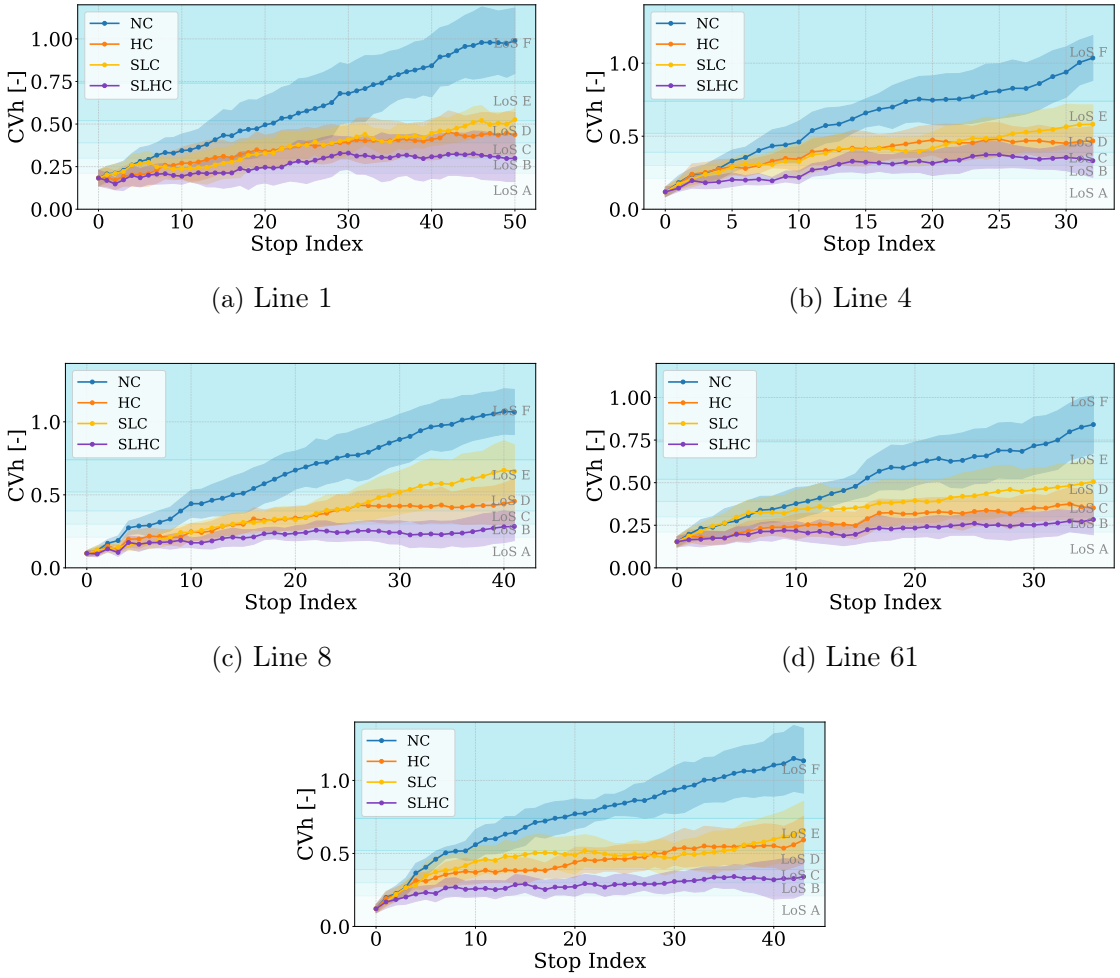


Figure 6: Speed limit control effect on energy consumption - a sample from Route 1, under identical traffic and demand conditions.



(a) Line 1

(b) Line 4

(c) Line 8

(d) Line 61

(e) Line 82

Figure 7: Coefficient of Variation of Headways (C_{vh}) per stop across the examined routes.

The evolution of service reliability along the route is illustrated through the coefficient of variation of headways C_{vh} in Fig. 7. Under NC, headway variability generally grows along the line and often reaches LoS F near the final stops. In contrast, all control strategies maintain more stable service, typically within LoS B–D. In most cases, SLHC yields the lowest and most stable C_{vh} values, consistent with the aggregate improvements observed in Fig. 5a.
Fig. 8 provides a complementary view using a time–space diagram for Line 1, showing that under NC, buses tend to bunch and may even overtake one another, while the control strategies maintain more regular spacing and mitigate these cascading effects.

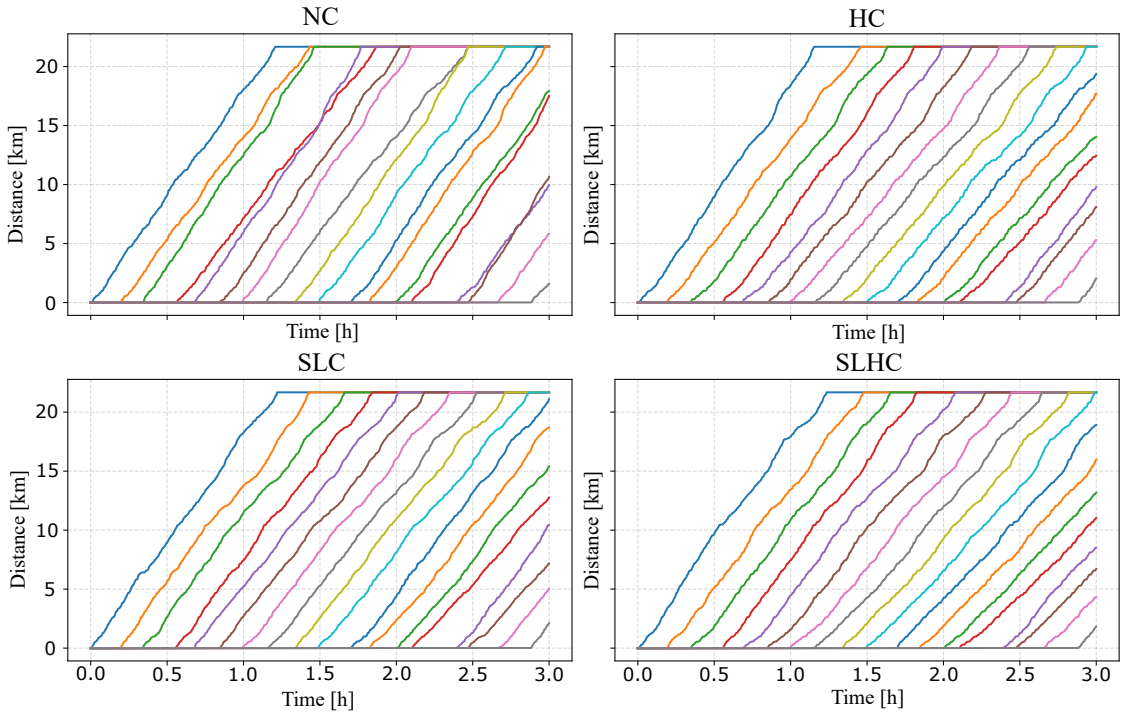
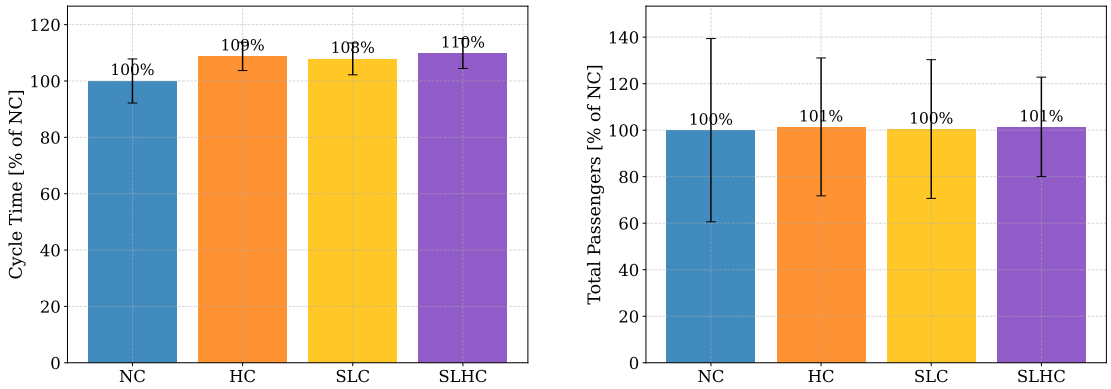


Figure 8: Time–space diagram of Line 1 under the four control strategies.

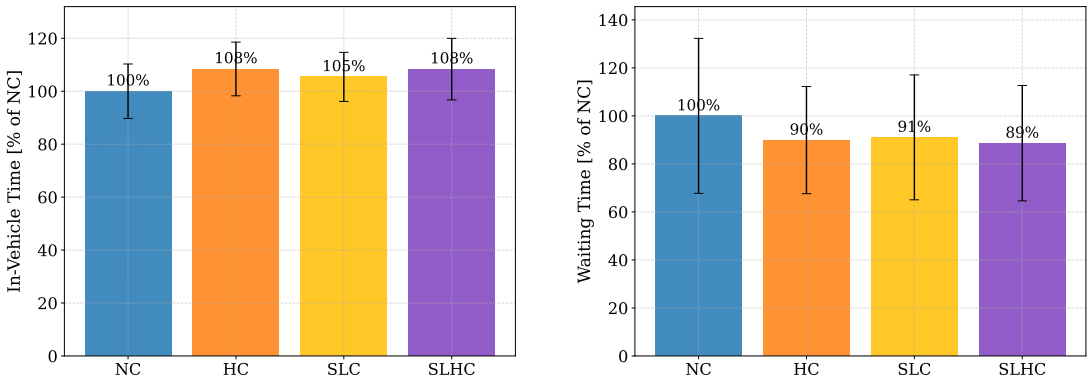
The control strategies also affect broader operational and passenger-oriented metrics. From the operator perspective, average running time increases by up to 10%, with holding contributing more to this increase than speed control. At the same time, the variability of running times decreases, indicating more stable operations. The average number of passengers served per trip remains essentially unchanged, although its variability is reduced, suggesting that control helps prevent crowding conditions associated with bunching.



(a) Average Running Time

(b) Total Boardings per Trip

Figure 9: Average running time and total boardings per trip, relative to the NC baseline.



(a) In-Vehicle Time per Passenger

(b) Waiting Time per Passenger

Figure 10: In-vehicle and waiting time per passenger relative to the NC baseline.

From the passenger perspective, control strategies slightly increase in-vehicle travel time due to holding and speed regulation, but also reduce waiting time through improved headway regularity (Fig. 10). Since waiting time is generally perceived as more burdensome than in-vehicle time (Van der Waard, 1988; Wardman, 2001, 2004), these results suggest that the control strategies may still improve perceived travel experience despite modest onboard delays.
Finally, Table 3 summarizes the average headway deviation and energy consumption results across all five lines under the full range of departure-irregularity scenarios defined in (22). Energy consumption remains highly stable across scenarios, whereas reliability improvements persist under HC and SLHC relative to NC. This indicates that the framework remains effective even as departure conditions become more irregular.

Table 3: Average results per scenario - % relative to NC

Scenario	**HW Error [%]**			**Energy Consumption [%]**		
	HC	SLC	SLHC	HC	SLC	SLHC
1	45	50	39	100	85	86
2	45	52	40	100	85	86
3	45	53	40	101	85	86
4	44	53	39	101	85	86
5	42	53	37	101	85	86
6	41	55	36	101	85	86
7	40	55	34	100	85	86
8	39	54	32	101	86	86
9	39	54	31	100	86	87
10	39	55	31	101	86	87

4 Conclusions

We presented a model-based, data-driven optimal control framework to improve the reliability and sustainability of bus operations. By integrating holding control at stops and speed-limit regulation between stops within an event-based MPC formulation, the proposed approach enables the joint regulation of time headways and fleet energy consumption under realistic operating conditions. The combined strategy SLHC consistently yielded the best outcomes across diverse conditions, achieving over 60% reduction in headway deviations from planned headway and about 15% decrease in energy consumption compared to the uncontrolled baseline. While headway regularity and energy efficiency improve substantially, moderate increases in travel time may occur. As such, real-world deployment should consider the trade-offs involved and tune the level of control to align with operational objectives and desired service levels. Overall, the findings demonstrate that jointly optimized, event-based control strategies can effectively enhance both service reliability and energy efficiency without relying on autonomous vehicle assumptions, supporting their applicability

in existing public transport systems.
Several extensions merit further investigation. First, integrating additional control levers, such as transit signal priority, could help mitigate the increases in travel time associated with delay-based strategies while preserving headway regularity. Second, extending the framework to other transit modes with higher right-of-way exclusivity, such as light rail or metro systems, may further enhance its effectiveness under more predictable operating conditions. Finally, improving the accuracy of short-term arrival and traffic-state prediction models could enhance the performance of horizon-based control, particularly under highly variable demand and congestion.

Acknowledgements

The research presented in this paper was funded by the Technion-Israel Institute of Technology and the Israeli Smart Transportation Research Center (ISTRC).

References

Anderson, P., & Daganzo, C. F. (2020). Effect of transit signal priority on bus service reliability. *Transportation Research Part B: Methodological*, *132*, 2–14.

Armenta-Déu, C., & Cortés, H. (2023). Analysis of kinetic energy recovery systems in electric vehicles. *Vehicles*, *5*(2), 387–403.

Asamer, J., Graser, A., Heilmann, B., & Ruthmair, M. (2016). Sensitivity analysis for energy demand estimation of electric vehicles. *Transportation Research Part D: Transport and Environment*, *46*, 182–199.

Associates, K. ., Administration, U. S. F. T., Program, T. C. R., & Corporation, T. D. (2003). *Transit capacity and quality of service manual* (Vol. 42). Transportation Research Board.

Borén, S. (2020). Electric buses' sustainability effects, noise, energy use, and costs. *International Journal of Sustainable Transportation*, *14*(12), 956–971.

Cao, Z., & Ceder, A. A. (2019). Autonomous shuttle bus service timetabling and vehicle scheduling using skip-stop tactic. *Transportation Research Part C: Emerging Technologies*, *102*, 370–395.

Ceder, A. (2016). *Public transit planning and operation: Modeling, practice and behavior*. CRC press.

Chen, W., Chen, Y., Wang, Y., & Fang, X. (2024). Bus drivers' behavioral intention to comply with real-time control instructions: An empirical study from china. *Sustainability*, *16*(9), 3623.

Christofa, E., & Skabardonis, A. (2011). Traffic signal optimization with application of transit signal priority to an isolated intersection. *Transportation Research Record*, *2259*(1), 192–201.

Cortés, C. E., Jara-Díaz, S., & Tirachini, A. (2011). Integrating short turning and deadheading in the optimization of transit services. *Transportation Research Part A: Policy and Practice*, *45*(5), 419–434.

Daganzo, C. (1997). *Fundamentals of transportation and traffic operations*. Pergamon.

Daganzo, C. F., & Pilachowski, J. (2011). Reducing bunching with bus-to-bus cooperation. *Transportation Research Part B: Methodological*, *45*(1), 267–277.

Delgado, F., Munoz, J. C., & Giesen, R. (2012). How much can holding and/or limiting boarding improve transit performance? *Transportation Research Part B: Methodological*, *46*(9), 1202–1217.

European Committee for Standardization (CEN). (2015). *Public transport — service interface for real-time information relating to public transport operations — part 1: Context and framework*. Standard EN 15531-1:2015.

Gallet, M., Massier, T., & Hamacher, T. (2018). Estimation of the energy demand of electric buses based on real-world data for large-scale public transport networks. *Applied energy*, *230*, 344–356.

Google and the GTFS Community. (2024). *Gtfs schedule reference.* `https://gtfs.org/documentation/schedule/reference/`. (Accessed: January 2025)

Henning, W. (2008). *Longitudinal dynamics of vehicles.* China Machine Press.

Heydari, S., Fajri, P., Lotfi, N., & Falahati, B. (2018). Influencing factors in low speed regenerative braking performance of electric vehicles. In *2018 ieee transportation electrification conference and expo (itec)* (pp. 494–499).

Ibarra-Rojas, O. J., Delgado, F., Giesen, R., & Muñoz, J. C. (2015). Planning, operation, and control of bus transport systems: A literature review. *Transportation Research Part B: Methodological*, *77*, 38–75.

Lacombe, R., Gros, S., Murgovski, N., & Kulcsár, B. (2020). Hierarchical control of electric bus lines. *IFAC-PapersOnLine*, *53*(2), 14179–14184.

Lacombe, R., Gros, S., Murgovski, N., & Kulcsár, B. (2021). Bilevel optimization for bunching mitigation and eco-driving of electric bus lines. *IEEE Transactions on Intelligent Transportation Systems*, *23*(8), 10662–10679.

Luethi, M., Weidmann, U., & Nash, A. (2007). Passenger arrival rates at public transport stations. In *Trb 86th annual meeting compendium of papers* (pp. 07–0635).

Newell, G. F. (2002). A simplified car-following theory: a lower order model. *Transportation Research Part B: Methodological*, *36*(3), 195–205.

Sirmatel, I. I., & Geroliminis, N. (2018). Mixed logical dynamical modeling and hybrid model predictive control of public transport operations. *Transportation Research Part B: Methodological*, *114*, 325–345.

Tang, J., Yang, Y., Hao, W., Liu, F., & Wang, Y. (2020). A data-driven timetable optimization of urban bus line based on multi-objective genetic algorithm. *IEEE Transactions on Intelligent Transportation Systems*, *22*(4), 2417–2429.

Tirachini, A. (2013). Bus dwell time: the effect of different fare collection systems, bus floor level and age of passengers. *Transportmetrica A: Transport Science*, *9*(1), 28–49.

Tuchner, A., & Haddad, J. (2017). Vehicle platoon formation using interpolating control: A laboratory experimental analysis. *Transportation Research Part C: Emerging Technologies*, *84*, 21–47.

UITP. (2017). *Urban public transport in the 21st century* (Tech. Rep.). -: Author.

Van der Waard, J. (1988). The relative importance of public transport trip time attributes in route choice. In *Ptrc summer annual meeting, 16th, 1988, bath, united kingdom.*

Van Oort, N. (2011). *Service reliability and urban public transport design.* Netherlands TRAIL Research School Delft, The Netherlands.

Varga, B., Tettamanti, T., & Kulcsár, B. (2019). Energy-aware predictive control for electrified bus networks. *Applied Energy*, *252*, 113477.

Wardman, M. (2001). A review of british evidence on time and service quality valuations. *Transportation Research Part E: Logistics and Transportation Review*, *37*(2-3), 107–128.

Wardman, M. (2004). Public transport values of time. *Transport policy*, *11*(4), 363–377.

Würtz, S., Bogenberger, K., Göhner, U., & Rupp, A. (2024). Towards efficient battery electric bus operations: A novel energy forecasting framework. *World Electric Vehicle Journal*, *15*(1), 27.

Xu, G., Li, W., Xu, K., & Song, Z. (2011). An intelligent regenerative braking strategy for electric vehicles. *Energies*, *4*(9), 1461–1477.

Xuan, Y., Argote, J., & Daganzo, C. F. (2011). Dynamic bus holding strategies for schedule reliability: Optimal linear control and performance analysis. *Transportation Research Part B: Methodological*, *45*(10), 1831–1845.

Yu, Q., Li, T., & Li, H. (2016). Improving urban bus emission and fuel consumption modeling by incorporating passenger load factor for real world driving. *Applied Energy*, *161*, 101–111.

Zhang, S., Wu, Y., Liu, H., Huang, R., Yang, L., Li, Z., ... Hao, J. (2014). Real-world fuel consumption and co2 emissions of urban public buses in beijing. *Applied Energy*, *113*, 1645–1655.

Zolfaghari, S., Azizi, N., & Jaber, M. Y. (2004). A model for holding strategy in public transit systems with real-time information. *International Journal of Transport Management*, *2*(2), 99–110.